

A Multiwalled-Carbon-Nanotube-Based Biosensor for Monitoring Microcystin-LR in Sources of Drinking Water Supplies

Changseok Han, Amos Doepke, Wondong Cho, Vlassis Likodimos, Armah A. de la Cruz, Tyson Back, William R. Heineman, H. Brian Halsall, Vesselin N. Shanov, Mark J. Schulz, Polycarpos Falaras, and Dionysios D. Dionysiou*

A multiwalled carbon nanotube (MWCNT)-based electrochemical biosensor is developed for monitoring microcystin-LR (MC-LR), a toxic cyanobacterial toxin, in sources of drinking water supplies. The biosensor electrodes are fabricated using vertically well-aligned, dense, millimeter-long MWCNT arrays with a narrow size distribution, grown on patterned Si substrates by water-assisted chemical vapor deposition. High temperature thermal treatment (2500 °C) in an Ar atmosphere is used to enhance the crystallinity of the pristine materials, followed by electrochemical functionalization in alkaline solution to produce oxygen-containing functional groups on the MWCNT surface, thus providing the anchoring sites for linking molecules that allow the immobilization of MC-LR onto the MWCNT array electrodes. Addition of the monoclonal antibodies specific to MC-LR in the incubation solutions offers the required sensor specificity for toxin detection. The performance of the MWCNT array biosensor is evaluated using micro-Raman spectroscopy, including polarized Raman measurements, X-ray photoelectron spectroscopy, cyclic voltammetry, optical microscopy, and Faradaic electrochemical impedance spectroscopy. A linear dependence of the electron-transfer resistance on the MC-LR concentration is observed in the range of 0.05 to 20 $\mu\text{g L}^{-1}$, which enables cyanotoxin monitoring well below the World Health Organization (WHO) provisional concentration limit of 1 $\mu\text{g L}^{-1}$ for MC-LR in drinking water.

1. Introduction

Harmful algal blooms (HAB) of cyanobacteria, known as blue-green algae, occur frequently in bodies of water worldwide as a consequence of eutrophication and global warming. Cyanobacterial HAB often produce undesirable color, odor, and tastes but most importantly, harmful toxins (cyanotoxins), such as hepatotoxins (microcystins (MCs), cylindrospermopsin, and nodularin), neurotoxins (anatoxins and saxitoxins), and dermatotoxins (lyngbyatoxins, lipopolysaccharides).^[1–6] Cyanobacteria and their highly potent toxins are a significant hazard for human health and the ecosystem in drinking water, recreational water, and aquaculture. Among the hepatotoxins, MCs are the most commonly reported group of cyanotoxins. Recently Graham et al.^[1] reported the presence of MCs in samples of cyanobacterial blooms (*Aphanizomenon*, *Cylindrospermopsis*, and *Microcystis*) from 23 eutrophic lakes in the midwestern United States.

C. Han, Prof. D. D. Dionysiou
Environmental Engineering and Science Program, School of Energy
Environmental, Biological and Medical Engineering
University of Cincinnati, Cincinnati, OH 45221-0012, USA
E-mail: dionysios.d.dionysiou@uc.edu

Dr. A. Doepke, Prof. W. R. Heineman, Prof. H. B. Halsall
Department of Chemistry, University of Cincinnati
Cincinnati, OH 45221-0172, USA

Dr. W. Cho, Prof. V. N. Shanov
Chemical Engineering, School of Energy
Environmental, Biological and Medical Engineering
University of Cincinnati, Cincinnati, OH 45221-0012, USA

Dr. V. Likodimos, Dr. P. Falaras
Institute of Advanced Materials, Physicochemical Processes
Nanotechnology and Microsystems (IAMPPNM)
Division of Physical Chemistry, NCSR Demokritos
15310 Aghia Paraskevi Attikis, Athens, Greece

Dr. A. A. de la Cruz
US EPA, Office of Research and Development
National Exposure Research Laboratory
Cincinnati, OH 45268, USA

Dr. T. Back
Air Force Research Laboratory
Materials and Manufacturing Directorate
Electronic and Optical Materials Branch (AFRL/RXPS)
Wright-Patterson AFB, OH 45433-7077, USA

Dr. T. Back
Universal Technology Corporation
1270 N. Fairfield Rd, Dayton, OH 45432, USA

Prof. M. J. Schulz
Mechanical Engineering and Mechanical Engineering Technology
School of Dynamic System, University of Cincinnati
Cincinnati, OH 45221-0072, USA

Prof. D. D. Dionysiou
Nireas-International Water Research Centre
University of Cyprus, 20537 Nicosia, Cyprus



DOI: 10.1002/adfm.201201920

Among MCs, microcystin-LR (MC-LR) is the most frequently occurring variant in the United States and throughout the world.^[7–10] The LD₅₀ and LC₅₀ value of MC-LR for mouse bioassay and brine shrimp assay are 25–150 μg kg⁻¹ and 5–10 mg L⁻¹, respectively.^[11] The provisional guideline concentration limit of 1 μg L⁻¹ MC-LR in drinking water was assigned by the World Health Organization (WHO).^[12] The development of reliable methods for monitoring MC-LR in water resources is of great interest to determine the occurrence and to prevent exposure to the toxin. Several methods have been developed to detect MC-LR, such as high-performance liquid chromatography/mass spectrometry (LC/MS),^[9,13] bioassays,^[14] biochemical assays,^[15] and immunoassays,^[13] which require long processing times, sophisticated instruments, complex procedures, or high processing cost^[16–19] and are in general used in the laboratory, not in situ. A sensitive, specific, simple, and rapid method for monitoring MC-LR could help to prevent exposure to the toxin. The unique physical and electrochemical properties (e.g., high electrical conductivity, ease of functionalization, high electrochemically active surface area, and broad range of working potentials in aqueous solutions) of carbon nanotubes (CNTs) make them a candidate material for developing electrochemical biosensors/immunosensors.^[20–25] A recent review from Singh et al.^[26] reported the advanced biosensors using single-walled CNTs and single-walled nanohorns showed good performance with high sensitivity, excellent stability, and fabrication reproducibility for the detection of MC-LR. Electrochemical biosensors using antibodies are also very promising for in situ monitoring of MC-LR due to the high selectivity, low cost, and simplicity of the detection method.^[10,27,28]

In this work we have developed a multiwalled CNT (MWCNT)-based biosensor for determination of MC-LR in water. The investigation was performed following three innovative approaches. First, dense arrays of millimeter-long, vertically aligned MWCNTs were synthesized from a patterned catalyst using water-assisted chemical vapor deposition (CVD). The MWCNT-based array electrodes were functionalized by electrochemical oxidation in an alkaline solution to produce oxygen-containing functional groups on the MWCNTs that were then coupled with linking agents followed by the subsequent immobilization of biomolecules. Second, MWCNT-based biosensors were prepared by conjugating MC-LR to the functionalized MWCNT array electrodes. Monoclonal antibodies specific to MC-LR in the incubation solutions had the required specificity to detect the toxin. The electron-transfer resistance of the functionalized MWCNT electrodes changed significantly after the MC-LR was conjugated and after exposure to antibodies in the incubation solutions, validating the biosensor performance. Finally, a calibration curve of the electron-transfer resistance versus the MC-LR concentration in the range of 0.05–20 μg L⁻¹ was established, permitting toxin detection well below the provisional MC-LR concentration limit in drinking water.

2. Results and Discussion

Figure 1 shows the cyclic voltammetric behavior of an MWCNT array electrode before and after functionalization, after potentiostatic treatment in 1.0 M NaOH solution. Before

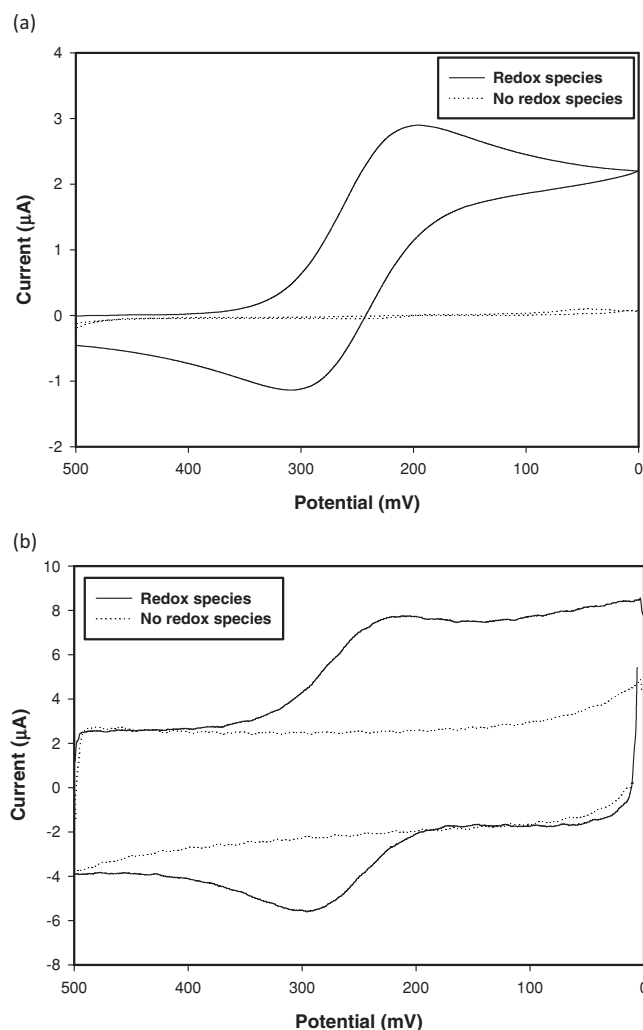


Figure 1. Cyclic voltammetry for MWCNT electrodes in 2 mM K₃[Fe(CN)₆]/0.5 M KNO₃: a) before functionalization and b) after functionalization.

functionalization, well defined reversible reduction/oxidation waves corresponding to the Fe^{III}/Fe^{II} redox couple were observed, which indicated efficient charge transfer between the MWCNTs and the electroactive species in solution (2 mM K₃[Fe(CN)₆]/0.5 M KNO₃) (see Figure 1a). After functionalization, an increase of the MWCNT electrode capacity controlled behavior was clearly observed due to the hydrolysis of the surface oxygen functional groups created on the MWCNTs by electrochemical oxidation in NaOH. The shape of the CV in the absence of Fe(CN)₆³⁻ redox-active species was rectangular and indicated a high specific capacitance of MWCNTs.^[29–33] The functionalized MWCNT electrodes exchanged electrons effectively in the presence of Fe(CN)₆³⁻, which indicated that they could be used as sensing materials.

Figure S1 (Supporting Information) summarizes the micro-Raman spectra of the pristine (control) and electrochemically functionalized MWCNT electrodes at 785 nm. The most characteristic feature commonly used as a probe of the successful

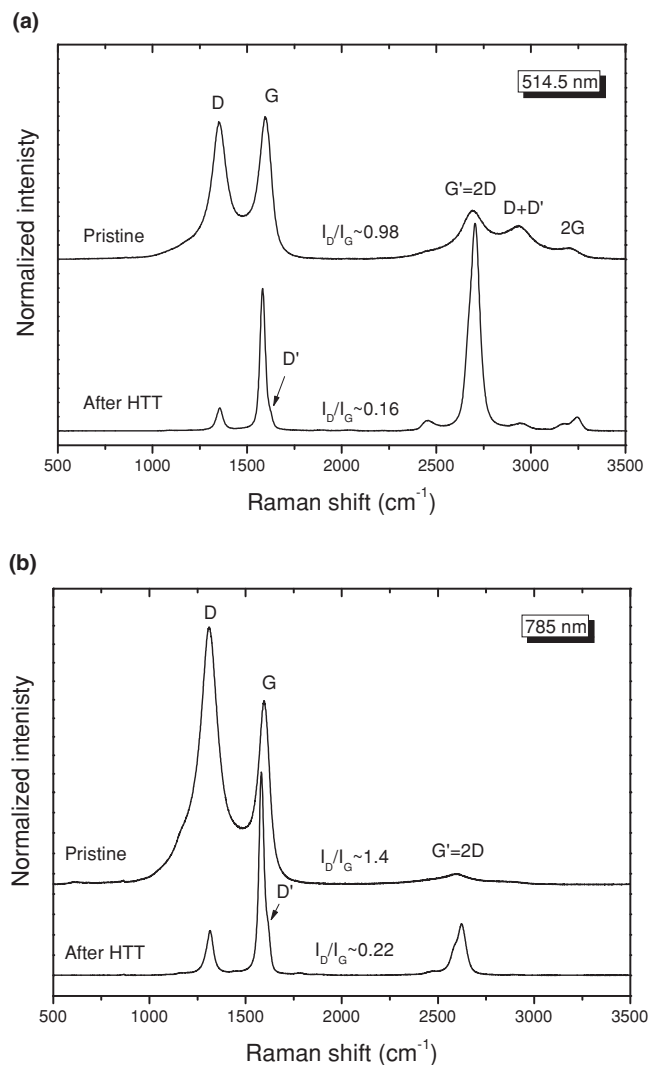


Figure 2. Micro-Raman spectra of the MWCNT electrodes before and after high temperature treatment at 514.5 nm (a) and 785 nm (b).

functionalization of the MWCNTs is the relative intensity of the defect-activated D band with respect to the tangential G band.^[34–36] As seen in Figure S1 (Supporting Information), both the D (1310 cm⁻¹) and G (1595 cm⁻¹) Raman bands of the MWCNTs were very broad and, most importantly, there was no appreciable or systematic variation of the relative intensity of the D-band to that of the G-band either between the functionalized tip and the interior of each electrode or between the functionalized tip and the control samples. This behavior can be rationalized by the inherently defective structure of MWCNTs produced by the catalytic CVD due to the relatively low growth temperature and the presence of soot-like amorphous carbon emerging as a pyrolysis by-product.^[37–39] These structural characteristics give rise to the broad Raman bands and the initially high I_D/I_G intensity ratio (≈ 2.5) that can effectively mask the effect of the functionalization treatment.

In order to improve the MWCNTs' crystallinity and structural order as well as their electrical conductivity,^[37,38,40] high

temperature annealing was done in an Ar atmosphere (an inert environment) at 2500 °C for 1 h. **Figure 2** compares the micro-Raman spectra of the control CNT electrodes after high temperature treatment (HTT) with the corresponding spectra of the pristine electrodes at both 785 and 514.5 nm excitation wavelengths. The HTT leads to a marked narrowing of the tangential G-band that downshifts to 1582 cm⁻¹ together with the narrowing and strong attenuation of the defect-activated D band and the clear identification of the D' band appearing as a shoulder to the G band at ≈ 1620 cm⁻¹ at both excitation wavelengths.^[34] This variation stems directly from the annealing of inherent structural defects that enhances the crystallinity of pristine MWCNTs upon graphitization. Accordingly, the intensity ratio I_D/I_G derived from the peak height of the D and G-bands is significantly reduced (an approximate six-fold decrease) at both excitations. In that case, application of the Tuinstra-Koenig relation $I_D/I_G = C(\lambda)/L$, where L is the in-plane crystallite size and $C(\lambda) = 4.4$ nm at 514.5 nm,^[34,41,42] indicates an increase of L from 4.5 nm for the pristine MWCNTs to 28 nm for the HTT ones. The high crystallinity of the HTT samples is further evidenced by the pronounced enhancement of the second order G' mode that stems from the first overtone of the D-band (2D) and the reduction of the relative intensity of the D + D' combination mode.^[36] In addition, the broad 2G band of the pristine samples evolved to two distinct peaks at 3178 and 3246 cm⁻¹ after HTT, which correspond closely to those reported for single-walled CNTs and graphite, respectively, confirming that MWCNTs form an intermediate structure. It is also worth noting that spectral analysis of the G'-band revealed the presence of two peaks for the HTT samples, especially at 785 nm. This is a characteristic feature of the 3D stacking order of highly oriented pyrolytic graphite (AB stacking of the hexagonal graphene *ab* planes along the *c*-axis of graphite), indicative of the structural transformation of MWCNTs upon HTT (i.e., a decrease of the interlayer spacing between the graphene shells of the MWCNTs approaching that of 3D graphite).^[37,38,40,43]

Figure 3a,b show the evolution of the Raman spectra for the electrochemically treated MWCNT electrodes at different NaOH concentrations at 514.5 and 785 nm excitations, respectively. The intensity (height) of the G-band has been normalized to unity for all samples. The relative intensity of the D-band to that of the G increases markedly with the NaOH concentration, verifying that the functionalization process is highly effective. The relative intensity of the D' and D + D' defect-activated modes increases accordingly, though to a lesser extent compared to the D band.^[36,44] The corresponding I_D/I_G intensity ratio, calculated from the relative peak heights of the D and G-bands, increases systematically as a function of the NaOH concentration, as shown in Figure 3c reaching the highest value at 1.0 M NaOH, in contrast to the pristine samples. Further evidence for the effectiveness of the functionalization process was obtained from polarized Raman measurements on the vertically aligned MWCNT electrodes. For this, polarization measurements were taken at 785 nm using a set of linear polarizers, a half-wave plate and a circular polarizer on the functionalized MWCNT electrodes. The corresponding backscattering geometry is schematically shown in **Figure 4a**, where k_i and k_s represent the propagating vectors of the incident and scattered laser beam along the Z-axis, and e_i and e_s are the incident and scattered

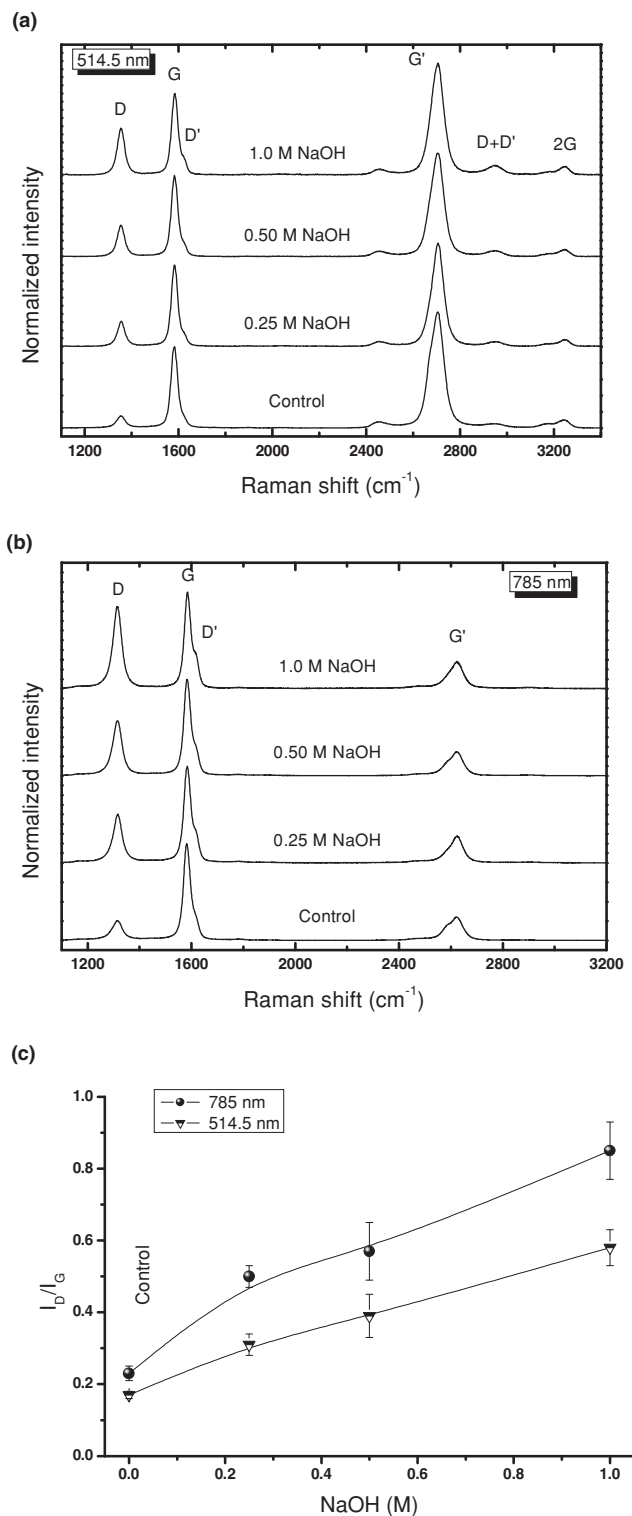


Figure 3. Micro-Raman spectra of the functionalized MWCNT electrodes in NaOH at a) 514.5 nm and b) 785 nm. c) Variation of the I_D/I_G intensity ratio as a function of the NaOH concentration at 514.5 and 785 nm.

polarization vectors, respectively, which can be mutually rotated in the horizontal (XY) microscope plane. Figure 4b–d are representative micro-Raman spectra of the control and two

functionalized electrodes with the Y axis being parallel to the nanotube axis. Both the defect-induced D and D' bands have considerable polarization dependence, though different from that of the tangential G mode. This behavior was independently confirmed by rotating the direction of MWCNT arrays by 90° so that the long tube axis lies along X on the microscope stage. In that case, the inverse relation between the (XX) and (YY) Raman spectra was recovered, verifying that the observed polarization dependence of the Raman bands is not due to any instrumental artifact. These results show that the origin of the D and D' bands is intrinsic to the functionalized MWCNTs and not due to the formation of amorphous carbon or even carbonaceous carbon fragments, created by the NaOH potential treatment that are not expected to yield appreciably polarized Raman bands. Moreover, the polarization dependence of the D and D' bands is quite different than that of the tangential G mode, resulting in significant variations of the I_D/I_G intensity ratio for the different polarizations. However, if the relative intensity of each band (G, D and D') is normalized to its maximum value, i.e., to the corresponding intensity of the (YY) spectra that was acquired with parallel (incident and scattered) polarizations along the MWCNT axis, then it is evidence that all intensities scale to approximately the same values for each polarization, independent of the I_D/I_G intensity ratio, i.e., independent of the amount of disorder introduced on the functionalized MWCNTs at different NaOH concentrations (Figure 5). This variation is in principle related to the different symmetry of each Raman mode, without excluding the presence of an antenna Raman effect.^[45] The average polarization dependence of the G-band, Figure 5d, resembles that reported for aligned MWCNTs of diameter ≈25 nm.^[46] On the other hand, the average polarization dependence of the D-band is less pronounced, and that of the D' band seems to lie between those of the G and D-bands, reflecting the difference in the symmetry of the defect activated modes.^[42]

The formation of oxygen-containing functional groups on the surface of the MWCNT electrode after functionalization was investigated by X-ray photoelectron spectroscopy (XPS). Figure 6c shows wide-scan survey spectra of the MWCNT before and after functionalization. The dominant O and C elements can be identified through the corresponding O1s and C1s peaks. The binding energies of C–C, C–O, C=O, and COO⁻ were detected at 284.4, 285.6, 287.2, and 289.0 eV in the C1s spectra, respectively. In the O1s binding region, the peaks of O=C, O–C, and H–O–H were observed at 531.7, 533.1, and 536.0 eV, respectively.^[47–51] The peaks of O1s and C1s increased due to the formation of oxygen-containing functional groups of the MWCNTs. Figure 6a,b show the chemical state of oxygen species on the surface of MWCNT before and after functionalization. The three peaks of O=C, O–C, and H–O–H in the O1s binding region clearly increased after functionalization. As shown in Figure 6d, the total concentration of oxygen increased from 9% to 25% atomic concentration after functionalization in 1.0 M NaOH solution, while the ratio of O–C to O=C in the O1s increased accordingly (from 1.13 to 1.56). These results were in good agreement with the results of Raman analysis, verifying the formation of functional groups on MWCNT upon electrochemical functionalization. Furthermore, a significant change of the wetting properties of the MWCNT array electrodes was

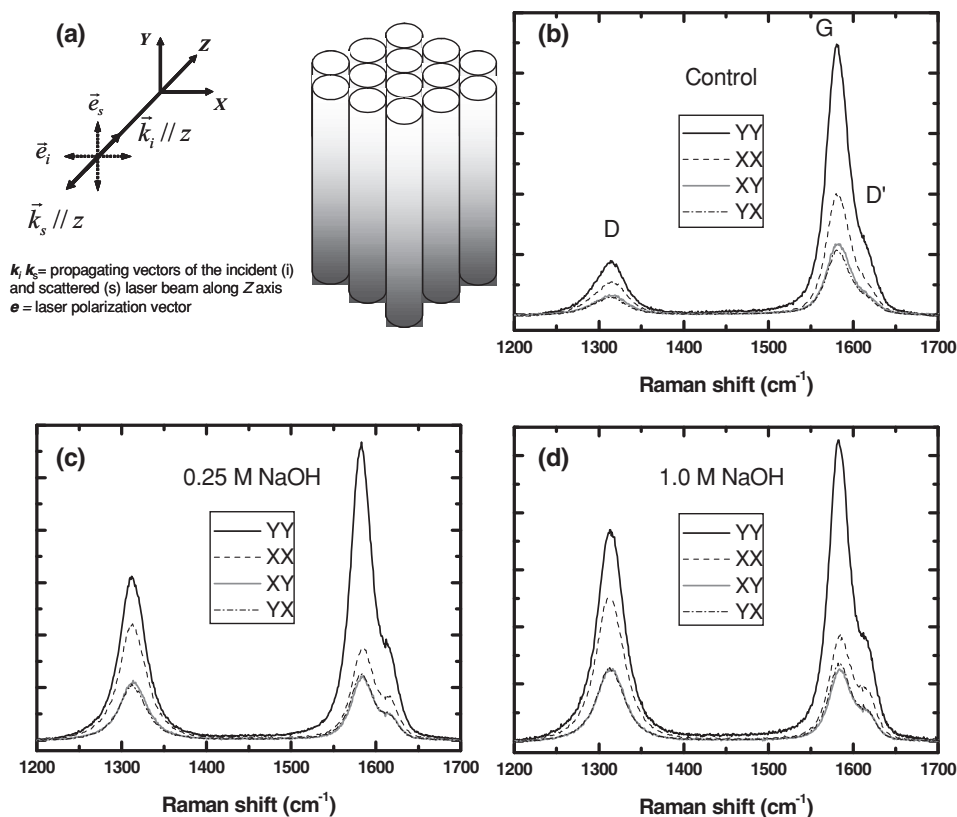


Figure 4. a) Raman backscattering polarization geometry on the aligned MWCNT arrays. b–d) Polarized micro-Raman spectra (using the 785 nm laser line) in parallel (YY), (XX), and cross-polarization (XY)-(YX) configurations for the control and two functionalized MWCNT electrodes at 0.25 and 1.0 M NaOH.

observed after functionalization. To visualize the variation of the hydrophilic character of the functionalized MWCNTs, the electrodes were dipped into MilliQ grade water. The cone-shaped depression was observed around the pristine MWCNT electrode due to the repulsion between the hydrophobic surface of the MWCNT array and the water. However, after NaOH electrochemical treatment, a bulging effect was observed, instead of the depression, due to the interaction between the functional groups and the water, indicating that MWCNTs became hydrophilic due to the formation of oxygen-containing functional groups on the surface of the functionalized MWCNT electrodes.^[52]

Figure S2 (Supporting Information) shows the Nyquist plots (Z_{imag} vs. Z_{real}) of the Faradaic electrochemical impedance spectra for the pristine and electrochemically functionalized MWCNT array electrodes in 1.0 M NaOH solution. After functionalization, the Faradaic electrochemical impedance decreased drastically due to the formation of oxygen-containing functional groups on the MWCNT electrodes that improved their surface hydrophilicity and wettability by the electrolyte (see Figure S3 in the Supporting Information).^[53] **Figure 7A** shows the Nyquist plots for the functionalized MWCNT electrode incubated in $5.0 \mu\text{g L}^{-1}$ MC-LR and antibody solution after conjugation with MC-LR. The observed Z_{imag} vs. Z_{real} spectra upon antibody/MC-LR anchoring are characteristic for Faradaic electrochemical impedance biosensors in the presence

of a redox couple, comprising a semicircle at higher frequencies that corresponds to the electron-transfer-limited process followed by a linear part at lower frequencies due to the diffusion-limited processes.^[54–56] In that case, attachment of the target biomolecules on the electrode surface is expected to reduce the available electrode area and hence retard interfacial electron-transfer. In addition, MC-LR on the electrode might be a retardant for the redox reaction as the presence of negative charges on both immobilized molecules and redox active species can increase the electron-transfer resistance due to electrostatic repulsion during approach of the redox active species to the electrode. This increase of the electron-transfer resistance is readily probed by the variation of the Nyquist plots. An increase of the semicircle diameter was indeed observed in the Nyquist plots (see Figure 7A: a–c) verifying the gradual increase of the electron-transfer resistance of the MWCNT array electrodes with the conjugation process using MC-LR and antibodies. Ramanavicius et al.^[57] also reported a significant increase in the real impedance due to the formation of the relatively larger protein complexes (Ppy/gp51/anti-gp51-antibody/secondary antibody) on the Ppy/gp51/anti-gp51 modified electrodes when the secondary antibodies were utilized to investigate the influence of larger protein complexes on electrochemical impedance spectroscopy (EIS). These results indicate that this technique using MWCNT array based biosensor is very effective for detecting MC-LR.

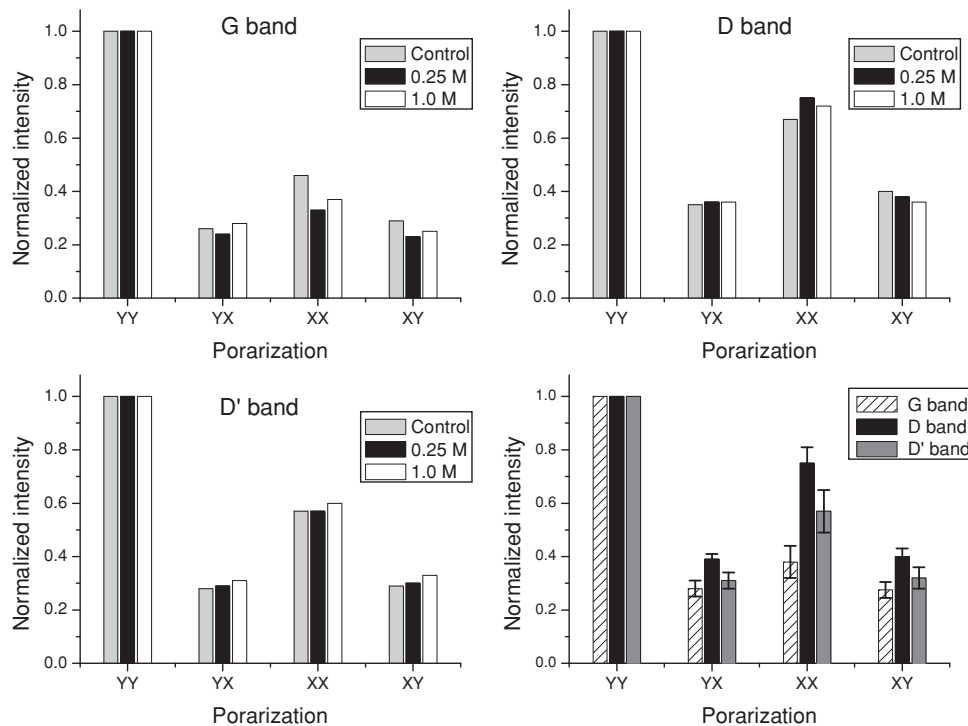


Figure 5. Polarization dependence of the G, D, and D' Raman band relative intensity for the control and two functionalized MWCNT electrodes (using the 785 nm laser line). The bottom right plot shows the average polarization dependence of the G, D and D' bands obtained by averaging the corresponding intensities for 12 functionalized MWCNT electrodes at different NaOH concentrations.

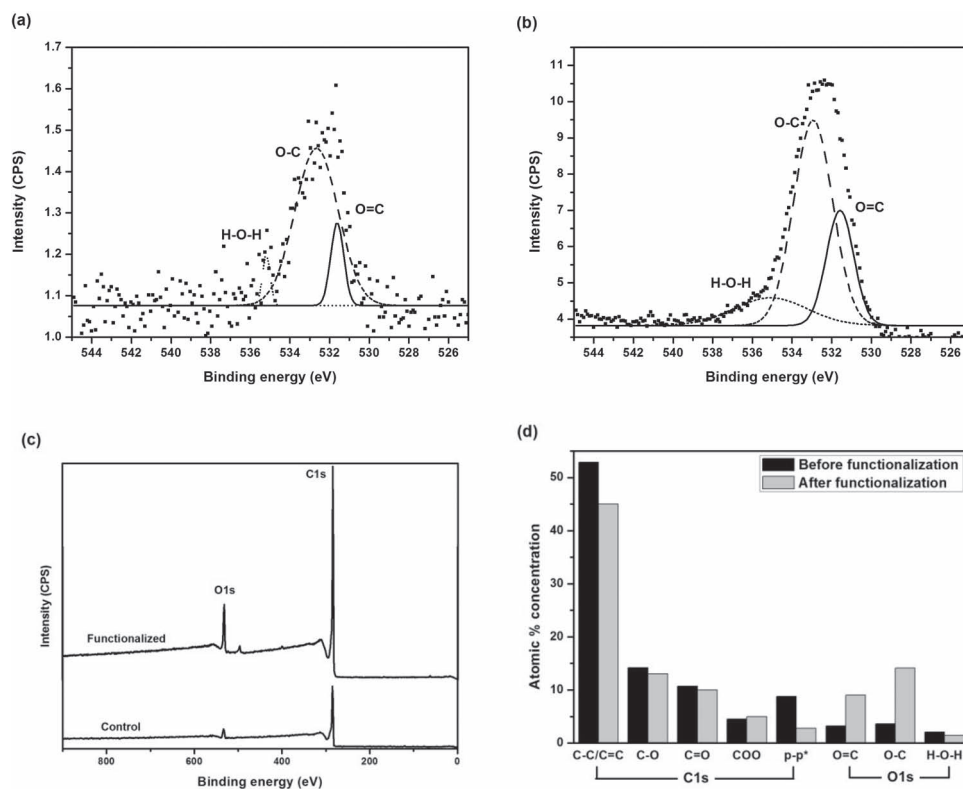


Figure 6. XPS analysis: O1s spectra of a) the control and b) the functionalized MWCNT electrode with 1.0 m NaOH solution. c) Wide-scan survey spectra and d) at% concentrations of carbon and oxygen containing surface groups before and after functionalization of the MWCNT electrode.

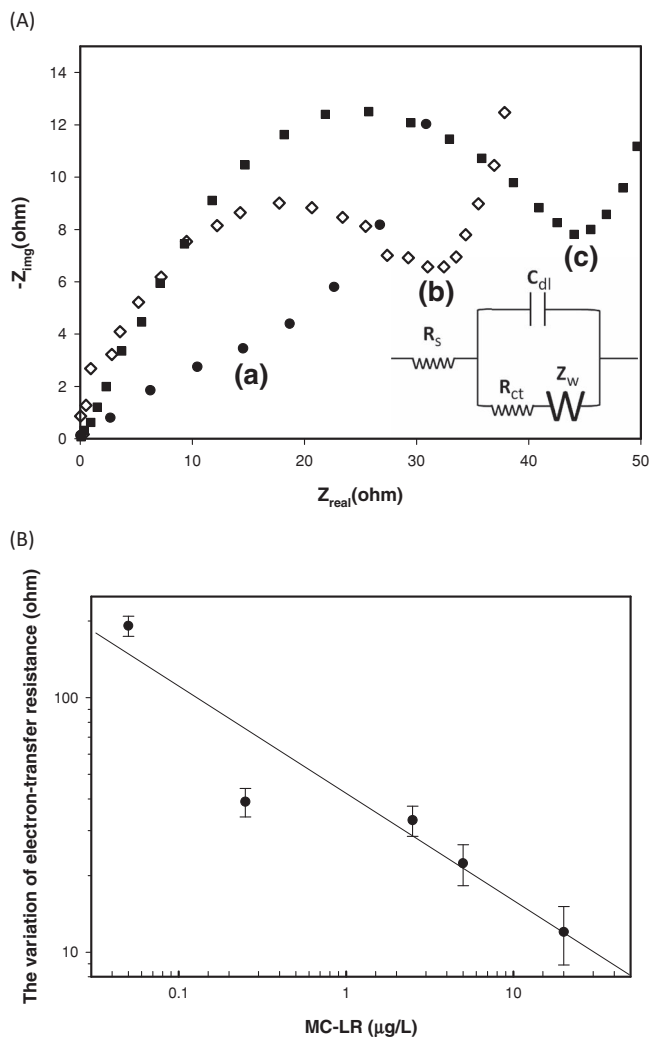


Figure 7. Nyquist Plots A) for Faradaic electrochemical impedance measurements in 5 mM $K_3[Fe(CN)_6]/K_4[Fe(CN)_6]$ with phosphate buffered saline (PBS): MWCNT array electrode after a) functionalization (1.0 M NaOH), b) MC-LR, and c) antibody conjugation; and the calibration curve B) for MWCNT-based biosensor based on the variation of the electron-transfer resistance with the MC-LR concentration in the range of 0.05–20 $\mu\text{g L}^{-1}$ in PBS.

Quantitation of the MWCNT array biosensor response for MC-LR detection was subsequently carried out by measuring the change of the electron-transfer resistance before and after conjugation of antibodies with different concentrations of MC-LR in the incubation solutions. A Randles model equivalent circuit, consisting of the solution resistance (R_s) in series with a parallel arrangement of the double layer capacitance (C_{dl}) and the electron-transfer resistance (R_{ct}) in series with Warbur impedance (Z_w), was used to interpret the behavior of the biosensors. The determined values of the R_{ct} are plotted using a logarithmic scale in Figure 7B as a function of the MC-LR concentration. Since the amount of antibodies was fixed and MC-LR concentration was varied, different amounts of unbound antibodies remained after the conjugation of MC-LR with antibodies. The remaining amount of unbound antibodies

in the solution after conjugation is thus inversely proportional to the concentration of MC-LR. Therefore, after the conjugation of remaining unbound antibodies with the MWCNT biosensor, the difference of electron-transfer resistance decreased (from 190 to 10 Ω) with the increase of the MC-LR concentration. The MWCNT biosensor had a linear response ($R^2 = 0.88$) between MC-LR concentrations from 0.05 to 20 $\mu\text{g L}^{-1}$ and the detection limit (s/n , s : standard deviation and n : the slope of calibration curve) was 0.04 $\mu\text{g L}^{-1}$, which is much lower than the WHO provisional guideline of 1 $\mu\text{g L}^{-1}$ for MC-LR.^[12] The inter- and intra-assay coefficients of variability were 13.1% and 7.8%, respectively, showing the acceptable fabrication reproducibility and the good repeatability of the method.

3. Summary and Conclusions

An extremely sensitive Faradaic electrochemical impedance biosensor for monitoring microcystin-LR in sources of drinking water supplies was developed using millimeter-long MWCNT arrays grown by water-assisted chemical vapor deposition with vertical alignment on catalytically patterned Si substrates. Scanning electron microscopy (SEM) and high-resolution transmission electron microscopy (HRTEM) analyses showed vertically well-oriented MWCNTs and well-defined, MWCNTs in the array. High temperature thermal treatment (2500 $^{\circ}\text{C}$) in an inert environment (Ar atmosphere) was exploited to anneal inherent structural defects and enhance the crystallinity of the pristine MWCNTs arrays. The MWCNT electrodes were functionalized by electrochemical oxidation in NaOH solution in order to produce oxygenated surface groups. A high degree of oxygen functionalization was achieved according to systematic cyclic voltammetry, micro-Raman spectroscopy, XPS, optical microscopy, and Faradaic EIS measurements. Specifically, cyclic voltammetry revealed well-defined redox peaks in the presence of redox species, while Faradaic EIS measurements showed a marked decrease of the Faradaic electrochemical impedance for the functionalized MWCNT arrays due to their improved wettability, directly evidenced by optical microscopy. Analysis of the Raman spectra showed the presence of oxygen-containing functional groups on the functionalized MWCNT electrodes after high temperature treatment by enhancing distinct defect-activated Raman bands as a function of the NaOH concentration. A significant increase of oxygen up to 25 at% concentration was determined by XPS analysis after the MWCNT electrodes were functionalized. The oxygenated surface groups provided the sites for linking agents and subsequent attachment of specific antibodies and toxin molecules. A two-step linking procedure enabled the immobilization of MC-LR onto the functionalized MWCNT array electrodes, and conjugation of monoclonal antibodies specific to MC-LR in the incubation solutions that provided the required specificity for detecting toxin. Validation and performance evaluation of the MWCNT array biosensor used Faradaic electrochemical impedance spectroscopy, which showed a clear increase of the electron-transfer resistance after MC-LR and antibody conjugation. A linear sensing response was thereby established over a wide MC-LR concentration range (0.05 to 20 $\mu\text{g L}^{-1}$) that allowed toxin detection well below the WHO provisional guideline limit of 1 $\mu\text{g L}^{-1}$ for MC-LR in drinking water.

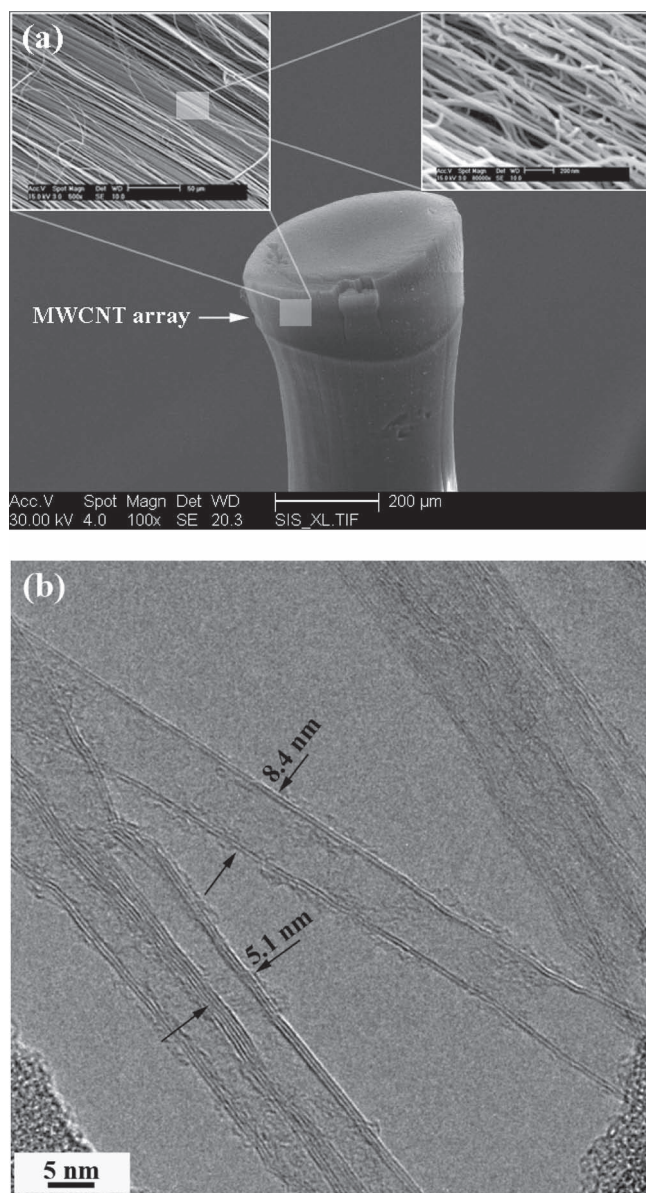


Figure 8. a) SEM image of the MWCNT electrode. The insets show individual MWCNTs in the array at high magnification. b) HRTEM image of as-grown MWCNTs.

4. Experimental Section

Reagents: NaOH, NaCl, KH_2PO_4 , $\text{Na}_2\text{HPO}_4 \cdot 7\text{H}_2\text{O}$, KNO_3 , EDC (1-ethyl-3-(3-dimethylaminopropyl) carbodiimide hydrochloride) and sulfo-NHS (*N*-hydroxysulfosuccinimide) were obtained from Thermo Fisher Scientific Inc. (Fair Lawn, NJ). $\text{K}_3[\text{Fe}(\text{CN})_6]$ and $\text{K}_4[\text{Fe}(\text{CN})_6]$ were obtained from J.T. Baker Company (Phillipsburg, NJ). MES hydrate (4-morpholinoethanesulfonic acid) was purchased from Acros Organics. Monoclonal antibodies specific to microcystins (ADDA specific, AD4G2, mouse IgG1) were obtained from ALEXIS Biochemicals. All solutions were prepared using MilliQ grade water having a resistivity of 18.2 megohm cm. All reagents were used as received.

Synthesis of MWCNT Arrays: MWCNT arrays 3–4 mm long were synthesized by a thermal CVD technique. An Easy Tube 3000 furnace, manufactured by CVD Equipment Corporation, was used for the CNT

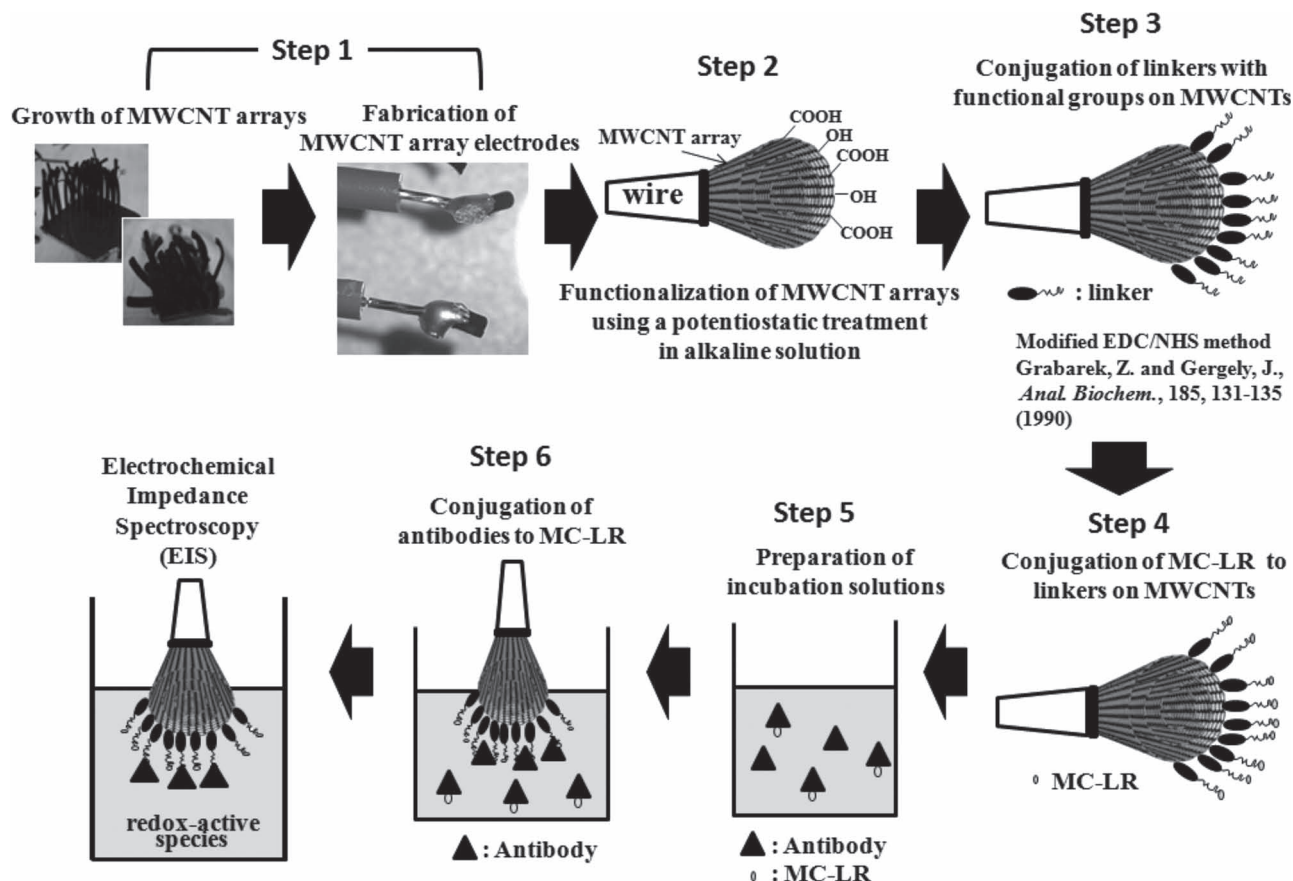
synthesis. A 15 nm thick film of Al_2O_3 was deposited on a Si wafer with a 500 nm thick oxide layer. A 1 nm thick Fe film was deposited on the Al_2O_3 layer; the Fe layer serves as a catalyst for the CNT nucleation and growth. All thin films were deposited by electron beam evaporation. Synthesis was performed at 750 °C, using C_2H_4 as a carbon source mixed with H_2 , Ar and a ppm amount of water vapor.

An MKS Quadrupole Mass Spectrometer, VISION 1000 P was used to monitor the gas composition of the growth zone. For the characterization of the MWCNTs, HRTEM (JEM-2010F (JEOL)) and SEM (Philips XL 30 ESEM-FEG) were employed (see Figure 8). The SEM image (Figure 8a) shows that the arrays consisted of dense vertically well-aligned MWCNTs. In addition, well defined multiwalled carbon nanotubes with diameters ranging from 5 to 9 nm are shown in an HRTEM image (Figure 8b). As displayed in this figure, the number of walls of the MWCNTs in the array was between 2 and 5.

Preparation of MWCNT Electrodes: The preparation of MMCNT electrodes consisted of six steps. In step one, the MWCNT arrays were connected to copper wire using conductive silver epoxy (M. G. Chemicals, Ontario, Canada) and dried for 24 h at room temperature. In step two, the tips of the MWCNT electrodes were electrochemically functionalized by applying a potential of 1.16 V vs. Ag/AgCl for 1 min, in NaOH (concentration range from 0.25 to 1.0 M)/0.5 M NaCl aqueous solutions. The functionalization potential was determined by comparing linear sweep voltammetry of MWCNT electrodes in 0.5 M KNO_3 and 1.0 M NaOH solutions. A potential of 1.16 V produced a significant current in 1.0 M NaOH but on the contrary, a very low current was observed in the case of 0.5 M KNO_3 supporting electrolyte.^[52]

In step three, zero-length cross-linkers were conjugated to the oxygen-containing functional groups on the surface of the MWCNT electrode. After electrochemically functionalizing the MWCNT arrays, a two-step zero-length cross-linking procedure using *N*-substituted carbodiimides and active esters was applied to enable further chemical derivatization of the electrodes with MC-LR.^[58] The electrodes were first incubated in a solution of 5 mM NHS in 0.1 M MES buffer, followed by a second incubation with 2 mM EDC in 0.1 M MES buffer. After the step three incubations, the electrodes were washed with 0.1 M MES buffer. In step four, MC-LR was conjugated to the MWCNT electrodes by 4 h incubation in 500 $\mu\text{g L}^{-1}$ of MC-LR in PBS buffer. In step five, the incubation solutions were prepared. A range of MC-LR concentrations were added to a fixed concentration of antibodies. The MC-LR concentration was from 0.05 to 20 $\mu\text{g L}^{-1}$ and the concentration of antibodies was 2.2 $\mu\text{g mL}^{-1}$. This solution was incubated for 30 min before determining the concentration of MC-LR. The remaining unbound antibodies in solution were inversely proportional to the amount of MC-LR. In step six, the biosensor was placed in the incubation solution. Any antibodies in solution that did not bind to the MC-LR in solution would now bind to the MC-LR on the electrode. **Scheme 1** shows the six sequential steps followed during the experimental procedure. The completed biosensors were then rinsed with H_2O and dipped into a potassium ferricyanide solution where the charge transfer resistance was determined using EIS. The change in R_{ct} is inversely proportional to the concentration of MC-LR in the incubation solutions in step 5.

Characterization of the MWCNT Electrode and Biosensor: The electrochemical properties of the MWCNT array electrodes were evaluated using cyclic voltammetry (BAS 100B electrochemical analyzer with BAS Epsilon EC and CV-27 potentiostats, Bioanalytical Systems Inc., USA) and electrochemical impedance spectroscopy (Gamry Potentiostat (Model: PCI4/750) with Gamry software (EIS3000)). The MWCNT electrodes were characterized by cyclic voltammetry (CV) in 2 mM potassium ferricyanide ($\text{K}_3[\text{Fe}(\text{CN})_6]$) solution using 0.5 M KNO_3 as the supporting electrolyte, with a Pt wire as auxiliary electrode and a Ag/AgCl electrode as the reference. Faradaic EIS measurements were with an open-circuit potential from 0.1 to 1×10^6 Hz, in a solution of 5.0 mM $\text{K}_4[\text{Fe}(\text{CN})_6]$ /5.0 mM $\text{K}_3[\text{Fe}(\text{CN})_6]$ prepared in PBS, pH 7.0. A Hitachi HV-C20 camera was used to visualize the variation of the wetting properties of the MWCNT array electrodes before and after functionalization. The physicochemical properties of the functionalized MWCNT electrodes were investigated by micro-Raman spectroscopy



Scheme 1. Preparation and detection procedure of MWCNT array biosensor for MC-LR.

using a Renishaw inVia Reflex microscope with a near infrared (NIR) diode laser ($\lambda = 785 \text{ nm}$) and an Ar⁺ laser at 514.5 nm as excitation sources. The laser beam was focused on the aligned MWCNTs by a 50 \times objective producing a laser spot size of $\approx 1 \mu\text{m}$ diameter, while the laser power was kept at low levels ($\approx 0.2 \text{ mW}/\mu\text{m}^2$) to avoid local heating. For each sample, the laser beam was focused on two different points: the first at the edge of the array with a few tens of micrometers from the edge of the electrode (tip), and the second, at the interior of the electrode (closer to the junction), corresponding to the sample area exposed (or not) to the NaOH solution (functionalized and non-functionalized), respectively. XPS (an SSI M-Probe XPS system) was used to investigate the formation of oxygenated surface groups after functionalization.

Supporting Information

Supporting Information is available from the Wiley Online Library or from the author.

Acknowledgements

This work was funded by the University of Cincinnati Internal Collaborative Award (INST) and the Ohio Water Resources Center through a grant from the USGS 104(b) program and the European Commission (Clean Water - Grant Agreement n^o 227017). Clean Water is a Collaborative Project co-funded by the Research DG of the European Commission within the joint RTD activities of the Environment and NMP Thematic Priorities. The work is also co-funded by the Cyprus Research

Promotion Foundation through Desmi 2009–2010, which was co-funded by the European Regional Development Fund and the Republic of Cyprus through the Research Promotion Foundation (Strategic Infrastructure Project NEAYΠIOΔOMH/ΣΤΡΑΤΗ/0308/09).

Received: July 10, 2012

Revised: September 6, 2012

Published online: November 9, 2012

- [1] J. L. Graham, K. A. Loftin, M. T. Meyer, A. C. Ziegler, *Environ. Sci. Technol.* **2010**, 44, 7361.
- [2] R. Agha, S. Cirés, L. Wörmer, J. A. Domínguez, A. Quesada, *Water Res.* **2012**, 46, 3043.
- [3] D. Pobel, J. Robin, J.-F. Humbert, *Water Res.* **2011**, 45, 1005.
- [4] W. Okello, C. Portmann, M. Erhard, K. Gademann, R. Kurmayer, *Environ. Toxicol.* **2010**, 25, 367.
- [5] Q. Wei, Y. Zhao, B. Du, D. Wu, Y. Cai, K. Mao, H. Li, C. Xu, *Adv. Funct. Mater.* **2011**, 21, 4193.
- [6] M. Pelaez, M. G. Antoniou, D. D. Dionysiou, A. A. de la Cruz, K. Tsimeli, T. Triantis, A. Hiskia, T. Kaloudis, C. Williams, M. Auel, A. Chapman, A. Foss, U. Khan, K. E. O'Shea, J. Westrick, in *Environmental Pollution* Vol. 16 (Eds: D. Fatta-Kassinos, K. Bester, K. Kümmerer), Springer Edited Series, New York **2010**, p. 101.
- [7] L. A. Lawton, H. Chambers, C. Edwards, A. A. Nwaopara, M. Healy, *Toxicol.* **2010**, 55, 973.
- [8] I. Maatouk, N. Bouaïcha, D. Fontan, Y. Levi, *Water Res.* **2002**, 36, 2891.

- [9] L. N. Sangolkar, S. S. Maske, T. Chakrabarti, *Water Res.* **2006**, *40*, 3485.
- [10] Y. Xia, J. Deng, L. Jiang, *Sens. Actuators B* **2010**, *145*, 713.
- [11] J. McElhiney, L. A. Lawton, *Toxicol. Appl. Pharm.* **2005**, *203*, 219.
- [12] World Health Organization, Guidelines for Drinking-Water Quality, 2nd ed. Addendum to Vol. 1. Recommendations, Geneva, World Health Organization **1998**, p. 13.
- [13] J. Rapala, K. Erkomaia, J. Kukkonen, K. Sivonen, K. Lahti, *Anal. Chim. Acta* **2002**, *466*, 213.
- [14] J. Kiviranta, K. Sivonen, S. I. Niemelä, *Environ. Toxicol. Water* **1991**, *6*, 423.
- [15] T. Ikehara, S. Imamura, N. Oshiro, S. Ikehara, F. Shinjo, T. Yasumoto, *Toxicol.* **2008**, *51*, 1368.
- [16] A. Zeck, M. G. Weller, R. Niessner, *Anal. Chem.* **2001**, *73*, 5509.
- [17] J. Meriluoto, *Anal. Chim. Acta* **1997**, *352*, 277.
- [18] B. Oudra, M. Loudike, V. Vasconcelos, B. Sabour, B. Sbiyyaa, K. Oufdou, N. Mezrioul, *Toxicology* **2002**, *17*, 32.
- [19] J.-H. Kim, B.-D. Yoon, H.-M. Oh, *Bull. Environ. Contam. Tox.* **2003**, *70*, 861.
- [20] C. Biswas, Y. H. Lee, *Adv. Funct. Mater.* **2011**, *21*, 3806.
- [21] G. Lai, J. Wu, H. Ju, F. Yan, *Adv. Funct. Mater.* **2011**, *21*, 2938.
- [22] Y. Y. Huang, E. M. Terentjev, *Adv. Funct. Mater.* **2010**, *20*, 4062.
- [23] S.-L. Gao, R.-C. Zhuang, J. Zhang, J.-W. Liu, E. Mäder, *Adv. Funct. Mater.* **2010**, *20*, 1885.
- [24] Y.-H. Yun, Z. Dong, V. N. Shanov, A. Doepke, W. R. Heineman, H. B. Halsall, A. Bhattacharya, D. K. Y. Wong, M. J. Schulz, *Sens. Actuators B* **2008**, *133*, 208.
- [25] M. S. Wang, L.-M. Peng, J. Y. Wang, Q. Chen, *Adv. Funct. Mater.* **2006**, *16*, 1462.
- [26] S. Singh, A. Srivastava, H.-M. Oh, C.-Y. Ahn, G.-G. Choi, R. K. Asthana, *Toxicol.* **2012**, *60*, 878.
- [27] J. Zhang, J. Lei, C. Xu, L. Ding, H. Ju, *Anal. Chem.* **2010**, *82*, 1117.
- [28] S. Dawan, P. Kanatharana, B. Wongkittisuksa, W. Limbut, A. Numnuam, C. Limsakul, P. Thavarungkul, *Anal. Chim. Acta* **2011**, *669*, 232.
- [29] J.-S. Ye, X. Liu, H. F. Cui, W.-D. Zhang, F.-S. Sheu, T. M. Lim, *Electrochem. Commun.* **2005**, *7*, 249.
- [30] C. G. Liu, H. T. Fang, F. Li, M. Liu, H. M. Cheng, *J. Power Sources* **2006**, *160*, 758.
- [31] F. Picó, J. M. Rojo, M. L. Sanjuán, A. Ansón, A. M. Benito, M. A. Callejas, W. K. Maser, M. T. Martínez, *J. Electrochem. Soc.* **2004**, *151*, A831.
- [32] K. H. An, W. S. Kim, Y. S. Park, J.-M. Moon, D. J. Bae, S. C. Lim, Y. S. Lee, Y. H. Lee, *Adv. Funct. Mater.* **2001**, *11*, 387.
- [33] K. H. An, W. S. Kim, Y. S. Park, Y. C. Choi, S. M. Lee, D. C. Chung, D. J. Bae, S. C. Lim, Y. H. Lee, *Adv. Mater.* **2001**, *13*, 497.
- [34] M. A. Pimenta, G. Dresselhaus, M. S. Dresselhaus, L. G. Cancado, A. Jorio, R. Saito, *Phys. Chem. Chem. Phys.* **2007**, *9*, 1276.
- [35] S. Osswald, M. Havel, Y. Gogotsi, *J. Raman Spectrosc.* **2007**, *38*, 728.
- [36] G. E. Romanos, V. Likodimos, R. R. N. Marques, T. A. Steriotis, S. K. Papageorgiou, J. L. Faria, J. L. Figueiredo, A. M. T. Silva, P. Falaras, *J. Phys. Chem. C* **2011**, *115*, 8534.
- [37] R. Andrews, D. Jacques, D. Qian, E. C. Dickey, *Carbon* **2001**, *39*, 1681.
- [38] Y. A. Kim, T. Hayashi, K. Osawa, M. S. Dresselhaus, M. Endo, *Chem. Phys. Lett.* **2003**, *380*, 319.
- [39] A. Rinaldi, B. Frank, D. S. Su, S. B. A. Hamid, R. Schlogl, *Chem. Mater.* **2011**, *23*, 926.
- [40] D. Mattia, M. P. Rossi, B. M. Kim, G. Korneva, H. H. Bau, Y. Gogotsi, *J. Phys. Chem. B* **2006**, *110*, 9850.
- [41] F. Tuinstra, J. L. Koenig, *J. Chem. Phys.* **1970**, *53*, 1126.
- [42] A. C. Ferrari, J. Robertson, *Phys. Rev. B* **2000**, *61*, 14095.
- [43] J. Chen, J. Y. Shan, T. Tsukada, F. Munekane, A. Kuno, M. Matsuo, T. Hayashi, Y. A. Kim, M. Endo, *Carbon* **2007**, *45*, 274.
- [44] C. Fantini, M. A. Pimenta, M. S. Strano, *J. Phys. Chem. C* **2008**, *112*, 13150.
- [45] V. Likodimos, T. Stergiopoulos, P. Falaras, J. Kunze, P. Schmuki, *J. Phys. Chem. C* **2008**, *112*, 12687.
- [46] A. M. Rao, A. Jorio, M. A. Pimenta, M. S. S. Dantas, R. Saito, G. Dresselhaus, M. S. Dresselhaus, *Phys. Rev. Lett.* **2000**, *84*, 1820.
- [47] T. I. T. Okpalugo, P. Papakonstantinou, H. Murphy, J. McLaughlin, N. M. D. Brown, *Carbon* **2004**, *43*, 153.
- [48] W. H. Lee, S. J. Kim, W. J. Lee, J. G. Lee, R. C. Haddon, P. J. Reucroft, *Appl. Surf. Sci.* **2001**, *181*, 121.
- [49] H. Hiura, T. W. Ebbesen, K. Tanigaki, *Adv. Mater.* **1995**, *7*, 275.
- [50] C. Mattevi, C. T. Wirth, S. Hofmann, R. Blume, M. Cantoro, C. Ducati, C. Cepek, A. Knop-Gericke, S. Milne, C. Castellarin-Cudia, S. Dolafi, A. Goldoni, R. Schloegl, J. Robertson, *J. Phys. Chem. C* **2008**, *112*, 12207.
- [51] S. Hofmann, R. Blume, C. T. Wirth, M. Cantoro, R. Sharma, C. Ducati, M. Hävecker, S. Zafeiratou, P. Schnoerch, A. Oestereich, D. Teschner, M. Albrecht, A. Knop-Gericke, R. Schlögl, J. Robertson, *J. Phys. Chem. C* **2009**, *113*, 1648.
- [52] A. Doepke, C. Han, T. Back, W. Cho, D. D. Dionysiou, V. Shanov, H. B. Halsall, W. R. Heineman, *Electroanalysis* **2012**, *24*, 1501.
- [53] X. Liu, Y. Wang, L. Zhan, W. Qiao, X. Liang, L. Ling, *J. Solid State Electron.* **2011**, *15*, 413.
- [54] B. Y. Chang, S.-M. Park, *Ann. Rev. Anal. Chem.* **2010**, *3*, 207.
- [55] L. Yang, R. Bashir, *Biotechnol. Adv.* **2008**, *26*, 135.
- [56] J.-Y. Park, S.-M. Park, *Sensors* **2009**, *9*, 9513.
- [57] A. Ramanavicius, A. Finkelsteinas, H. Cesulius, A. Ramanaviciene, *Bioelectrochemistry* **2012**, *79*, 11.
- [58] Z. Grabarek, J. Gergely, *Anal. Biochem.* **1990**, *185*, 131.